Neuroscience 212 (2012) 190–200

REPEATED LONGITUDINAL *IN VIVO* IMAGING OF NEURO-GLIO-VASCULAR UNIT AT THE PERIPHERAL BOUNDARY OF ISCHEMIA IN MOUSE CEREBRAL CORTEX

K. MASAMOTO,[a,b] Y. TOMITA,[c] H. TORIUMI,[c] I. AOKI,[b] M. UNEKAWA,[c] H. TAKUWA,[b] Y. ITOH,[c] N. SUZUKI[c] AND I. KANNO[b]*

[a] *Center for Frontier Science and Engineering, University of Electro-Communications, 1-5-1 Chofugaoka, Chofu, Tokyo 182-8585, Japan*

[b] *Molecular Imaging Center, National Institute of Radiological Sciences, 4-9-1 Anagawa, Inage, Chiba 263-8555, Japan*

[c] *Department of Neurology, School of Medicine, Keio University, 35 Shinanomachi, Shinjuku, Tokyo 160-8582, Japan*

Abstract—Understanding the cellular events evoked at the peripheral boundary of cerebral ischemia is critical for therapeutic outcome against the insult of cerebral ischemia. The present study reports a repeated longitudinal imaging for cellular-scale changes of neuro-glia-vascular unit at the boundary of cerebral ischemia in mouse cerebral cortex *in vivo*. Two-photon microscopy was used to trace the longitudinal changes of cortical microvasculature and astroglia following permanent middle cerebral artery occlusion (MCAO). We found that sulforhodamine 101 (SR101), a previously-known marker of astroglia, provide a bright signal in the vessels soon after the intraperitoneal injection, and that intensity was sufficient to detect the microvasculature up to a depth of 0.8 mm. After 5–8 h from the injection of SR101, cortical astroglia was also imaged up to a depth of 0.4 mm. After 1 day from MCAO, some microvessels showed a closure of the lumen space in the occluded MCA territory, leading to a restructuring of microvascular networks up to 7 days after MCAO. At the regions of the distorted microvasculature, an increase in the number of cells labeled with SR101 was detected, which was found as due to labeled neurons. Immunohistochemical results further showed that ischemia provokes neuronal uptake of SR101, which delineate a boundary between dying and surviving cells at the peripheral zone of ischemia *in vivo*. Finally, reproducibility of the MCAO model was evaluated with magnetic resonance imaging (MRI) in a different animal group, which showed the consistent infarct volume at the MCA territory over the subjects.

Key words: MRI, two-photon microscopy, sulforhodamine, chronic cranial window, fluorescent imaging, cerebral microcirculation.

INTRODUCTION

Cerebral ischemia-provoked damages on the central nervous system (CNS) vary depending on the gradients of ischemia from a core to a peripheral region (del Zoppo and Mabuchi, 2003; del Zoppo, 2010). In particular, it is believed that disturbance on the CNS cells near the peripheral boundary of ischemia is reversible. To better understand the cellular events elicited at the ischemic boundary zone is therefore critical to develop a therapeutic technique and improve the resultant prognosis against the insult of cerebral ischemia.

In the cerebral cortex, cortical microvasculature is closely associated with surrounding astroglia (i.e., gliovascular unit), which has been shown to play a key role in maintaining the CNS homeostasis (Abbott et al., 2006; Mathiisen et al., 2010). In response to evoked neural activity, astroglia acts on cerebral arterioles through an interface made up of astroglial endfeet and vascular smooth muscle cells (Straub and Nelson, 2007; Carmignoto and Gómez-Gonzalo, 2010). Depending on oxygen availability, astroglia release either vasodilatory or vasoconstrictory signals to adjust cerebral microcirculation (Gordon et al., 2008). These studies highlight the pivotal role of the gliovascular unit in balancing activity-dependent energy demand and supply. However, little is known about the functional role of gliovascular unit in response to the insult of cerebral ischemia in which energy supply-demand balances were disrupted.

In the present study, to explore the role of the gliovascular unit at the peripheral zone of cerebral ischemia, we developed a method for longitudinal cellular imaging with two-photon microscopy in *in vivo* mouse cerebral cortex. Two-photon imaging was repeatedly performed to trace the cellular-scale changes of cortical microvasculature and astroglia following permanent middle cerebral artery occlusion (MCAO) (Toriumi et al., 2009). We used sulforhodamine 101 (SR101), a previously known fluorescent marker of astroglia (Nimmerjahn et al., 2004; Kafitz et al., 2008; McCaslin et al., 2011), as a multiple-labeling agent for the repeated imaging. A previous report showed that sulforhodamine is permeable to blood–brain barrier (Vérant et al., 2008). Here, we found that intraperitoneal injection of SR101 allows for labeling astroglia, microcirculation, and neurons at the ischemic boundary,

*Corresponding author. Tel: +81-43-206-4716; fax: +81-43-206-0819.
E-mail address: kanno@nirs.go.jp (I. Kanno).

Abbreviations: CNS, central nervous system; GFP, green fluorescent protein; IP, intraperitoneal; MRI, magnetic resonance imaging; MCAO, middle cerebral artery occlusion; NA, number of averages; ROI, region of interest; SR101, sulforhodamine 101.

0306-4522/12 $36.00 © 2012 IBRO. Published by Elsevier Ltd. All rights reserved.
http://dx.doi.org/10.1016/j.neuroscience.2012.03.034

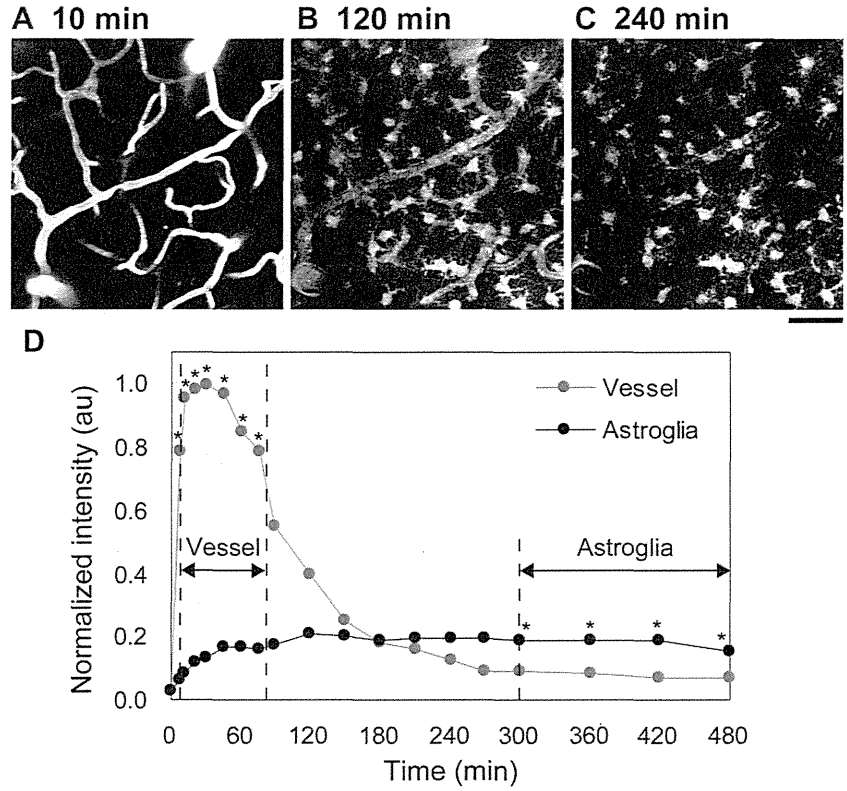

Fig. 1. Time-lapse imaging of cortical microvasculature and astroglia after intraperitoneal injection of SR101. The fluorescent signals were initially detected in the vessels and subsequently shifted to astroglia. The images (upper panels) represent a maximum intensity projection obtained from a depth of 155–210 μm (a total of 12 images) captured 10 min (A), 120 min (B), and 240 min (C) after the injection of SR101. Scale bar = 50 μm. (D) A normalized mean time–intensity curve ($N = 4$ animals) demonstrated an optimum time-window for imaging the individual structures over 10–80 min and 300–480 min following SR101 injection for vessels (gray) and astroglia (black), respectively (*$P < 0.05$).

depending on time and space after the injection. To determine the optimum time-window for imaging the individual structures, a time–intensity curve was measured in cortical microvasculature and astroglia following the injection of SR101. Then, the method was applied to transgenic mice in which endothelial cells were genetically engineered with Tie2-green fluorescent protein (GFP) (Motoike et al., 2000), to further demonstrate the feasibility of long-term tracking of neuro-glio-vascular unit at the ischemic boundary zone. Immunohistochemical analysis was also performed to verify the specificity of SR101 labeling. Finally, magnetic resonance imaging (MRI) was used to determine the reproducibility of infarct volume created by MCAO in separate animal groups.

EXPERIMENTAL PROCEDURES

Animal preparation

Animal use and experimental protocols were approved by the Institutional Animal Care and Use Committee. Two separate animal groups of male C57BL/6J mice (6–21 weeks; Japan SLC, Inc., Shizuoka, Japan) were used for two-photon imaging ($N = 4$) and MRI ($N = 5$), respectively. In two-photon imaging experiments, a time–intensity curve of injected SR101 fluorescent signal was measured. Nine STOCK Tg[Tie2-GFP]287Sato/J mice (6–12 weeks; The Jackson Laboratory, Bar Harobor, ME) (Motoike et al., 2000; Itoh et al., 2010) were further used for MCAO experiments. In this experiment, MCAO that was modified from Tamura's original method (Tamura et al., 1981; Toriumi et al., 2009) was conducted in five animals, whereas sham-operation (without occlusion but received the same operation) was performed in other four animals. Briefly, the permanent occlusion was made at the proximal branch of the MCA for MCAO group, whereas the only skull was drilled but no occlusion was made for the sham group. During the surgery, rectal temperature of the animal was monitored and maintained (37 °C) with a heating pad (BWT-100, BRC, Nagoya, Japan), and no detectable changes of systemic blood pressure due to the surgical procedure were ensured by means of non-invasive blood pressure monitor (MK2000ST, Muromachi Kikai, Co. Ltd., Tokyo, Japan). The MCAO procedure was implemented with the assumption that vascular pattern and response to MCAO were similar in both C57BL/6J and Tie2-GFP animal groups.

Two-photon imaging experiment

The animals were initially anesthetized with isoflurane (2–3%) and a custom-made attachment device for holding the head was fixed on the skull (Takuwa et al., 2011). A closed cranial window was made by removing a part of the skull (4 mm in diameter) over the left somatosensory cortex while leaving the dura intact, and the exposed cortex was sealed with a cover glass (Tomita et al., 2005). The animal was then allowed to recover from anesthesia and was housed in a cage with free access to food and water. The animals were also kept in the cage in between scheduled experiments. On each experimental day, SR101 (MP Biomedicals, Irvine, CA) dissolved in saline (5–10 mM) was injected intraperitoneally (8 μL/g body weight) to the animal just before beginning the imaging experiments. The animal was placed on a custom-made apparatus (Takuwa et al., 2011) under 1% isoflurane, and the imaging was conducted with a two-photon

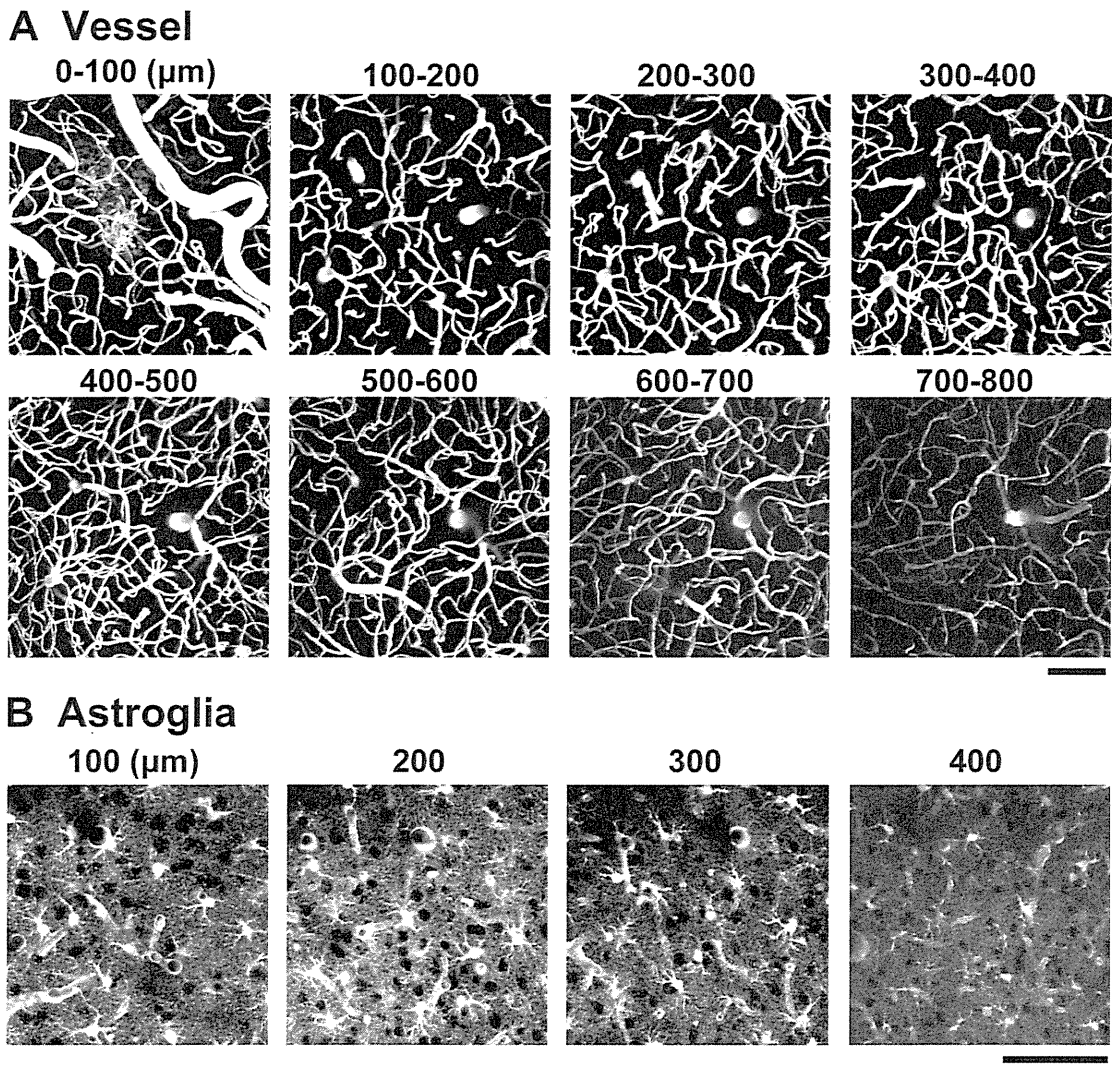

Fig. 2. Depth imaging of cortical microvasculature and astroglia. The images of microvasculature was detected up to 0.8 mm from the cortical surface (A), whereas the astroglia was 0.4 mm. (B) For visualization purposes, a maximum intensity projection was performed for vessel images obtained over each 100-μm depth (21 images), whereas the astroglia image was represented with a single slice (one image). Scale bar = 100 μm.

microscope (TCS-SP5MP, Leica Microsystems GmbH, Wetzlar, Germany) excited at 900 nm. An emission signal was separated by a beam splitter (560/10 nm) and simultaneously detected through a band-pass filter for SR101 (610/75 nm) and GFP (525/50 nm). A single image plane consisted of 1024 by 1024 pixels and the in-plane pixel-size was 0.25–0.45 μm depending on an instrumental zoom factor. Volume images were acquired up to a maximum depth of 0.4–0.8 mm from the cortical surface with a z-step size of either 4 or 5 μm (Park et al., 2008). For measurement of a time–intensity curve, a volume image was acquired in a single location in each animal every 5–60 min for 8 h from the onset of SR101 injection. For the MCAO mice, pre-MCAO imaging was conducted 4 days prior to the operation, and follow-up imaging was performed at the same locations. In each animal, a total of 7–16 locations were investigated across the cortical regions of middle to anterior cerebral arterial supply.

All volume images obtained were reconstructed and analyzed offline with LAS AF software (Leica Microsystems GmbH, Wetzlar, Germany). Fluorescent signal intensity was measured by averaging all pixel data within a region of interest (ROI) set with a circle 5 μm in diameter. For the measurements of time–intensity curves, vessel and astroglia ROIs were manually selected around the center of the microvessels (< 10 μm in diameter) and astroglial soma, respectively. A total of 22 vessels and 24 astroglia ROIs were obtained from four animals. A mean time–intensity curve was then measured and normalized to the peak value in each animal. For the MCAO experiments, a number of labeled cells around the ischemic boundary was counted using volume-reconstructed images ($100 \times 100 \times 200\ \mu m^3$), and the density was reported. For this specific analysis, half of each image that contained distorted microvessels was selected among all measured locations. Student's *t*-test was performed, and statistical significance was reported ($P < 0.05$). Data were presented as mean ± standard deviation.

Immunohistochemistry

Immunohistochemistry was performed in a Tie2-GFP mouse ($N = 2$) in which no cranial window was made. At day 4 after MCAO, SR101 was intraperitoneally injected, and perfusion fixation with 4% paraformaldehyde was performed 4 h after the injection of SR101. The brain was removed, and a 15-μm-thick coronal section including the somatosensory cortex was incubated with antibodies against neuronal nuclei (1:200, Ms anti-NeuN, Millipore, Billerica, MA) and glial fibrillary acidic protein (1:500, Ms anti-GFAP [GA5], mAb, Cell Signaling Technology, Boston, MA).

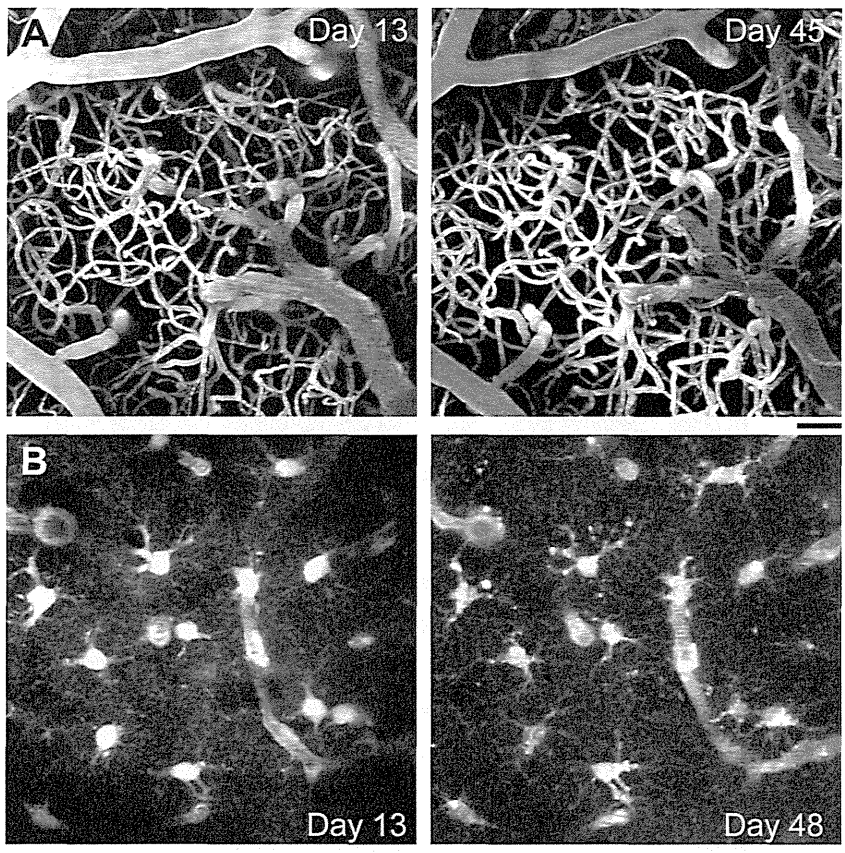

Fig. 3. Long-term imaging of cortical microvasculature and astroglia. Identical imaging protocols were repeatedly performed up to 7 weeks after the attachment of cranial window. In this period, a total of 3–7 imaging sessions were conducted at identical locations ($N = 5$ animals). The representative images of microvasculature (A) and astroglia (B) were taken on days 13 (left) and 45 or 48 (right) after the attachment of cranial window. For visualization purposes, a maximum intensity projection was performed for images obtained over depths of 0–300 μm (61 images) for vessels and 45–55 μm (3 images) for astroglia. Reproducible images were consistently obtained in all five animals, and thus indicating the minimum invasiveness of two-photon imaging to the measured cortex. Scale bar = 50 μm.

MRI experiments

All MRI experiments were performed on a 7.0 T horizontal MRI scanner (Magnet: Kobelco and JASTEC Japan; Console: Bruker Biospin, Germany) with a volume coil for transmission (Bruker) and 2-ch phased array surface coil for reception (Mice brain coil, Rapid Biomedical, Germany). The mice were initially anesthetized with 3.0% isoflurane (Forane, Abbott Japan, Japan), orally intubated, and then ventilated with 2.0% isoflurane and 1:5 oxygen/room-air-mixture using a rodent ventilator (MRI-1, CWE, Ardmore, PA). Rectal temperature was continuously monitored and maintained at 37.0 ± 0.5 °C using a heating pad (Temperature control unit, Rapid Biomedical) throughout all experiments. During MRI scanning, the mice lay in a prone position on a MRI compatible cradle and held in place by handmade ear bars. The first imaging slices were carefully set at rhinal fissure with reference to the mouse brain atlas (Paxinos and Franklin, 2004). Each image set consisted of five different kinds of MRI measurements performed in the following order: T_1-weighted imaging (T_1WI, slice offset = 0 mm), T_1W (slice offset = 0.8 mm), T_2- and diffusion-weighted MRI (T_2WI and DWI, slice offset = 0 mm), T_2WI and DWI (slice offset = 0.8 mm), and 3D MR angiography.

T_1-weighted MRI. Transaxial T_1WI using multi-slice spin echo (SE) sequence (TR/TE = 300/9.6 ms, slice thickness = 0.8 mm, slice gap = 0.8 mm, Fat-Sup = on, matrix = 256 × 170, field of view = 19.2 × 12.8 mm^2, number of averages (NA) = 8, number of slices = 7, slice offset = 0 or 0.8 mm, and scan time = 6 min 48 s) were acquired at 1, 3 and 7 days after the MCAO. Frequency-selective saturation pulses and crusher magnetic field gradients were used for the fat suppression.

T_2- and diffusion-weighted MRI. Transaxial T_2WI and DWI were acquired using a multi-slice SE sequence (TR/TE = 3600/70 ms, slice thickness = 0.8 mm, slice gap = 0.8 mm, Fat-Sup = on, matrix = 256 × 170, field of view = 19.2 × 12.8 mm^2, slice orientation = transaxial (same slice position as the T_1WI), NA = 1, b value = 0 (T_2-weighted imaging) or 1000 (DWI) s/mm^2, diffusion direction = z, and scan time = 15 min 21 s).

MR angiography. MR angiography was performed using a 3D-FLASH sequence to compare the condition of the vascular system (TR = 15 ms, TE = 2.5 ms, flip angle = 20°, field-of-view (FOV) = 25.6 × 12.8 × 12.8 mm^2, matrix = 256 × 128 × 128, and scan time = 12 min 17 s). Maximum intensity projection was calculated from the 3D MR angiography using ParaVision software (Ver. 5.1, Bruker Biospin).

Measurement of infarct volume. The infarct volume in the MCAO animals was calculated manually using Image-J software (NIH). First, an area of each hemisphere was calculated for all T_2-weigthed images scanned over whole coronal sections taken 1 day after MCAO. Then, infarct area was manually determined in each image with contrast-adjustment to maintain similar ranges

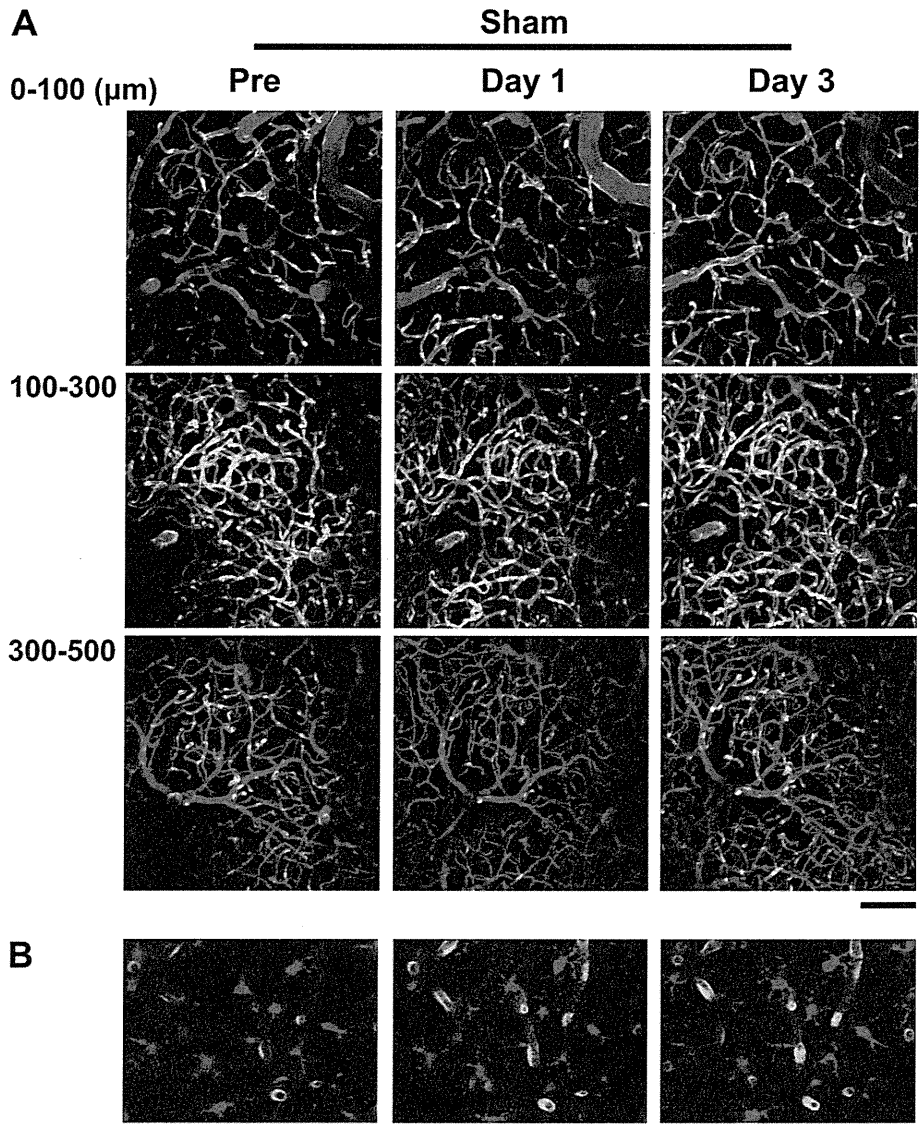

Fig. 4. Two-photon imaging of cortical microvasculature and astroglia in sham-operated animal. (A) The images represent cortical microvasculature with Tie2-GFP (green) and SR101 (red) in a single location measured over depths of 0–100 μm, 100–300 μm, and 300–500 μm (from top to bottom) at pre-, post-operation 1, and 3 days (left to right). A maximum intensity projection was performed. Scale bar = 100 μm. (B) Imaging of gliovascular unit with Tie2-GFP expressed endothelium (green) and astroglia labeled with SR101 (red). The representative single-slice image was captured at a depth of 100 μm at pre-, post-operation 1, and 3 days (left to right). The representative images showed that an identical structure was maintained for both cortical microvasculature and astroglia. Scale bar = 50 μm. (For interpretation of the references to color in this figure legend, the reader is referred to the web version of this article.)

of the intensity levels across the different sections and animals. Finally, the infarct volume was calculated by correcting the volume change of diseased hemisphere relative to a normal side.

RESULTS

Time–intensity curve measurements

A fluorescent signal appeared in the vessels about 5 min after the intraperitoneal injection of SR101 (Fig. 1A). The signals reached a peak 20–30 min after the injection, and then weakened over time. At the same time, a faint signal was detected in the extravascular space 40–60 min after the injection, which became recognizable as the shape of astroglia (Fig. 1B, C). The mean time–intensity curve showed statistically significant differences between vessel and astroglia ROIs over 10–80 min and 300–480 min after the injection (Fig. 1D). For extended periods, the fluorescent signal in the astrocyte was gradually decreased, and a half-life period was measured as 1 day after the injection. In contrast, 1 day after the injection the signal of SR101 in the bloodstream was not detectable (i.e., an intensity equivalent to the noise level), indicating an exclusion of SR101 from the body. Based on this result, the following experiments were performed at 10–80 min for vessel and 300–480 min for astroglia imaging after the intraperitoneal injection of SR101, respectively. With this optimized time-window, the cortical microvasculature was detected up to a depth of 0.8 mm from the cortical surface (Fig. 2A), whereas the astroglia was a depth of 0.4 mm in our experimental condition

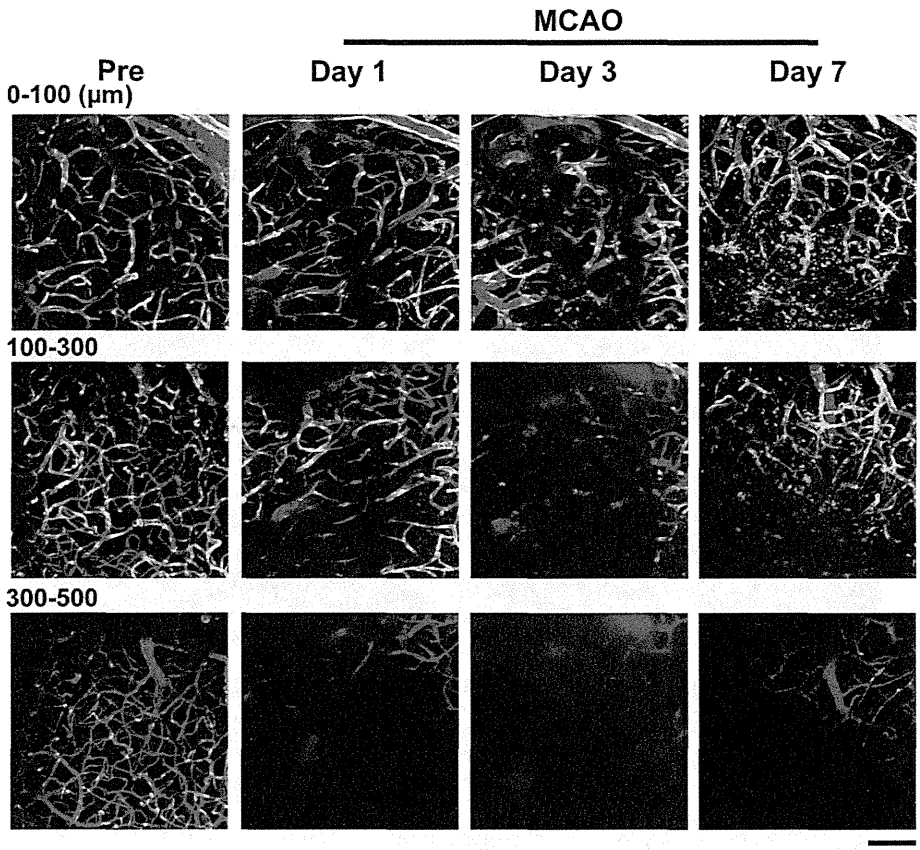

Fig. 5. Two-photon imaging of cortical microvasculature in MCAO animal. The images represent progressive changes of microvasculature measured repeatedly in a single location over depths of 0–100 μm, 100–300 μm, and 300–500 μm (from top to bottom) at pre-MCAO, post-MCAO 1, 3, and 7 days (left to right). A maximum intensity projection was performed. Vessel labeled with SR101 (red) generally showed deeper penetration of the signals compared to the vessel imaged with GFP (green). Deformation of pre-existing vessels was seen in the visualized upper part of the images on days 1–3. At day 1, some microvessels were labeled only with GFP, indicating an incomplete perfusion of SR101. Dilation of capillaries was also seen in this period, but which later became stabilized, and changes in the vascularity were seen on day 7. In deep tissue, vessels were poorly visualized on days 1 and 3, possibly due to no perfusion (i.e., limited delivery of fluorescent agent) in these regions and/or changes in tissue optical properties due to the brain edema. Also, blurred vessel structure suggested a leakage of SR101, which could be due to impaired brain–blood barrier. Scale bar = 100 μm. (For interpretation of the references to color in this figure legend, the reader is referred to the web version of this article.)

(Fig. 2B). We further confirmed that the imaged microvasculature and astroglia shape were consistently maintained over extended periods of the repeated longitudinal imaging experiments (Fig. 3A, B). In addition, follow-up measurements of the animal's body weight showed average 0.1–1.0 g increase every week after the injection of SR101, which was in good agreement with those (0.16 ± 0.47 g increase per week) of the normal animals (i.e., without administration of SR101, $N = 13$).

Two-photon imaging in MCAO mice

In the sham-operated mice, the identical structure was demonstrated for both cortical microvasculature (Fig. 4A) and astroglia (Fig. 4B) across pre-, 1 day and 3 days after the surgical operation. In the MCAO mice, topographic structures of the microvascular networks were distorted 1 day after MCAO (Fig. 5). Some microvessels showed only GFP signals, but not SR101, indicating an incomplete perfusion in the MCA territory regions at day 1 after the MCAO (Fig. 5). Dilation and regression of the microvessels were observed near the area of distorted microvasculature 3 days after MCAO, but these vessels were restructured until 7 days after MCAO (Fig. 5). In this paper we defined the regions that showed a boundary between damaged and undamaged microvascular areas in the periphery of MCA territory as "peripheral boundary" (Fig. 6A). In these regions, not the whole microvessels were occluded and thus delivery of SR101 can be maintained by neighboring microvessels that were survived following ischemia.

For the astroglia imaging, rounded and swelled structures were seen in regions where the microvasculature was distorted after MCAO. In a period of 1 through 3 days after MCAO, a cluster of the cells (5–7 μm in a diameter) that were newly labeled with SR101 was detected (Fig. 6B). The cluster was located around the periphery of the ischemic region (Fig. 6A). At 8 days after MCAO, the labeled cells were not detectable in the peripheral zone. At this moment, morphologically activated astroglia surrounded the ischemic boundary and their processes extended toward the core of ischemia (Fig. 6C).

A number of cells labeled with SR101 significantly ($P < 0.05$ vs. pre-MCAO) increased 1–3 days after MCAO

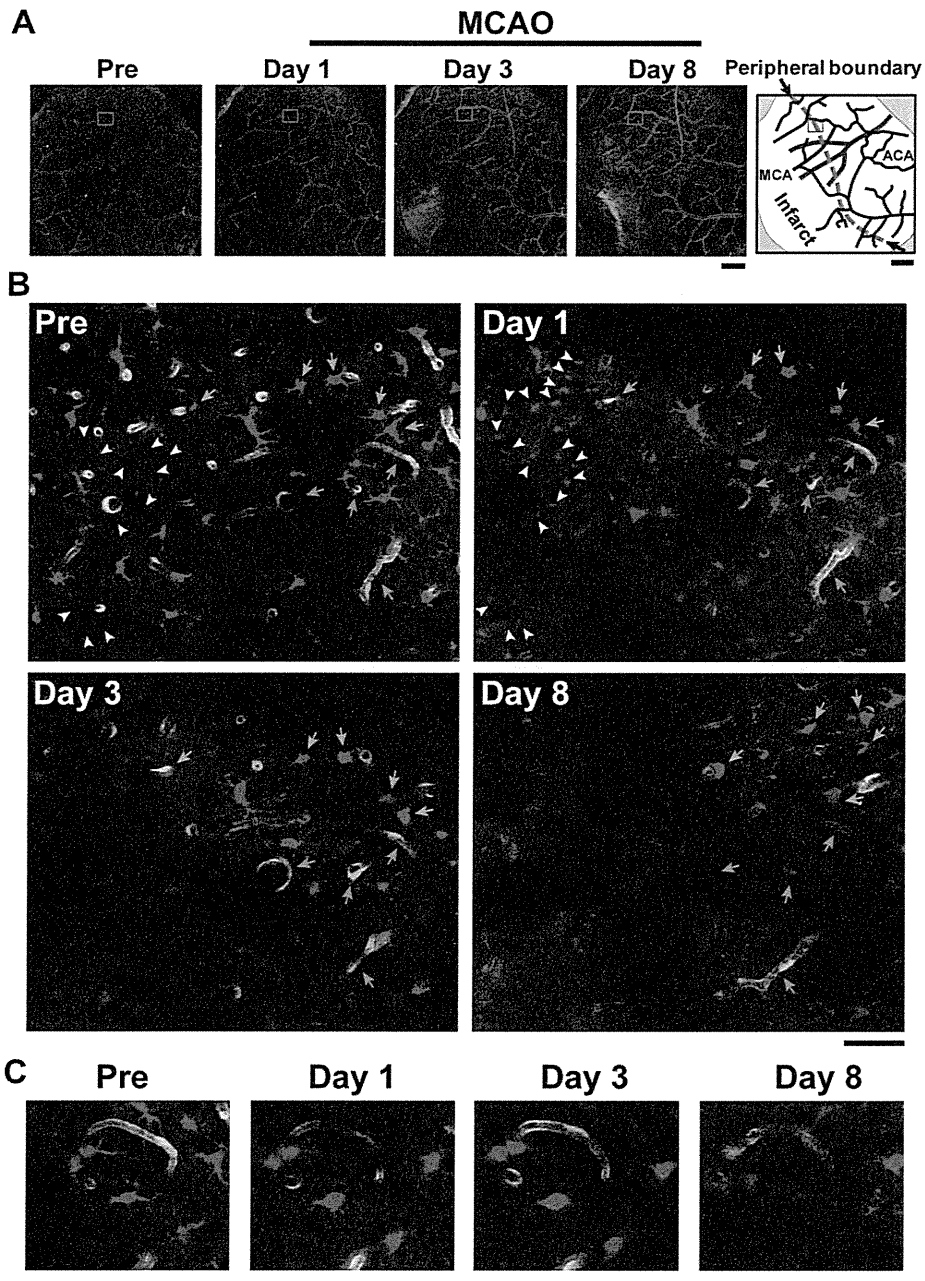

Fig. 6. Two-photon imaging of gliovascular unit in the ischemic boundary zone. (A) Vessel pattern of cortical surface in GFP mouse. In the MCA territory (a left side of the image), GFP-labeled arterial networks were progressively distorted after MCAO, whereas the other side of the vessel networks was relatively preserved (a right side of the image). The observed ischemic boundary based on the microscopic imaging of cortical microvasculature and cells were depicted (right). The cortical regions of the MCA territory became infarct, whereas the area around a meeting point of MCA and ACA developed a peripheral boundary. A blue and red color in the image indicates pial artery and vein, respectively. The rectangular region represents the location for detailed two-photon imaging shown in (B). Scale bar = 500 μm. (B) Two-photon imaging of gliovascular unit. The images represent a single slice image (a depth of 80 μm), captured at pre-MCAO, and 1, 3, and 8 days post-MCAO. In the pre-MCAO image, astroglia labeled with SR101 (red arrows) extended their endfeet to nearby vessels labeled with Tie2-GFP (green arrows). Rounded cells not labeled with SR101 (black spots) were diffusely observed (yellow arrow head). At day 1, typical astroglia disappeared in the left part of the image. Unlabeled small round cells also decreased in number whereas round cells labeled with SR101 were seen to emerge in the left half of the images (white arrowhead) from days 1–3. None of the cells or vessels were detectable on the proximal side of the ischemic lesion on day 8. In the peripheral region, microvessels were more densely surrounded by astroglial endfeet (right half) of the image on day 8. Scale bar = 50 μm. A higher magnification image was shown in (C). Scale bar = 20 μm. (For interpretation of the references to color in this figure legend, the reader is referred to the web version of this article.)

relative to the pre-MCAO conditions; 1.4 ± 0.1, 1.9 ± 0.6, and $1.9 \pm 0.9 \times 10^4$ cells/mm^3 at pre-, day 1, and day 3 after MCAO, respectively (Fig. 7B), whereas the sham-operated mice showed a consistent number of the labeled cells; 1.3 ± 0.2, 1.3 ± 0.1, and $1.4 \pm 0.2 \times 10^4$ cells/mm^3 at pre-, day 1, and day 3 after sham

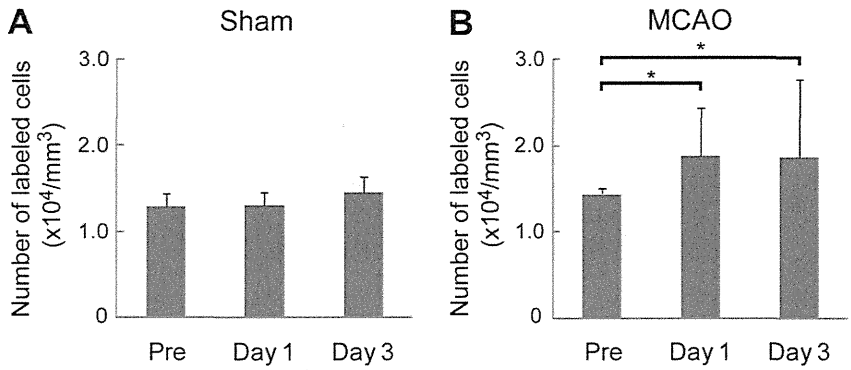

Fig. 7. The density of cells labeled with SR101. A number of labeled cells that were greater than 5 μm in size were seen in the images of the $100 \times 100 \times 200\ \mu m^3$ volume in sham-operated control groups (A) and the ischemic boundary in MCAO groups (B). Statistically significant increases in labeled cells relative to pre-MCAO were observed on days 1 and 3 post-MCAO, whereas no significant changes over this period was seen in the sham-operated groups. Error bar: standard deviation ($N = 4$ animals). $^*P < 0.05$ (student's t-test, against pre-operation conditions).

operation, respectively (Fig. 7A). In the MCAO groups, no apparent decrease of the number of labeled astrocytes was confirmed within the measured ROIs, as compared to the pre-MCAO conditions. Immunohistochemical results further showed that the newly labeled cells were co-localized with cells positive for NeuN (Fig. 8), indicating the ischemia-induced neuronal uptake of SR101. In the undamaged normal areas, cells labeled with SR101 were positive for GFAP (Fig. 8), which showed SR101 uptake by only astroglia in normal regions.

MRI experiments with MCAO

The signal changes in the occluded side of the cortex was detected in both T_2WI and DWI 1 day after MCAO, which was consistent over a period of the experiments up to 7 days from MCAO (Fig. 9). No signal changes were evident in the sham-operated animal (Fig. 9). The mean infarct volume in the MCAO animals was $33.5 \pm 4.8\ mm^3$. The MCA was certainly occluded (5/5) and no reflow in the occluded side of MCA was seen in MR angiography images.

DISCUSSION

The present study demonstrated a stable and reproducible method for repeated long-term imaging of neuroglio-vascular unit using two-photon microscopy with SR101. Unlike MRI, two-photon imaging requires labeling of the targets with specific fluorescent dye. For imaging microcirculation, a stable contrast agent that is retained in the blood circulation with a sufficient amount of fluorescence is needed. This was generally achieved with intravenous (IV) injection of a fluorescent marker that consists of a macromolecule and bioinert water-soluble materials (Kleinfeld et al., 1998; Seylaz et al., 1999), fluorescent microbeads (Rovainen et al., 1993), or fluorescently labeled red blood cells collected from donor animals (Sarelius and Duling, 1982). On the other hand, labeling of astroglia *in vivo* has been conducted via topical application of dye to the cortex or direct injection into the parenchymal tissue (Nimmerjahn et al., 2004; McCaslin et al., 2011). However, these conventional methods potentially disturb cortical microcirculation because the injection requires the exposure, puncture, or removal of the dura in order to access the parenchymal cells. Because minimum invasiveness is critical for reproducible long-term imaging, alternative ways of labeling using fluorescent proteins have been proposed as promising methods to endogenously label astroglia (Zhuo et al., 1997; Shannon et al., 2007). However, genetically engineered methods are limited to specific animals. The application of fluorescent proteins in other animal models requires the construction of further hybrids or breeding, which is time-consuming and costly.

In the present study, we found that SR101, a widely used fluorescent marker for astroglia (Nimmerjahn et al., 2004; Kafitz et al., 2008; McCaslin et al., 2011), can be used as a multiple-labeling agent for longitudinal imaging astroglia, microcirculation, and ischemic cellular-boundaries. Administration of a blood plasma marker using intraperitoneal (IP) injection offers great advantage in terms of its technical ease and capability of wide applications, such as for infants and disease models in which the vessels are extremely difficult for catheterization. A similar approach to that used in this paper was reported in a recent paper that showed that IV injection of sulforhodamine B allows for labeling of both cortical microcirculation and astroglia (Vérant et al., 2008). The present approaches with IP injection of SR101 extended these previously published methods and may further allow for unlimited labeling of cortical astroglia and microcirculation for most diseases and genetically engineered animals.

The depth penetration for imaging of vessels labeled with SR101 was slightly deeper than that reported in our previous study of the rat cortex using water soluble Quantum dot with thinned skull preparation that allowed microvascular imaging up to 0.6 mm (Park et al., 2008). This difference could be due to the use of different animal species (mice vs. rats) and/or window preparation techniques (cranial window vs. thinned skull). We also observed that the microvasculature imaged with SR101 provided deeper penetration relative to that of the GFP labeling. This is due to the fact that a longer wavelength in visible light provides better penetration in biological tissue. Also, we observed 0.8-mm penetration for microvasculature, but 0.4 mm for astroglia labeled with SR101. The difference

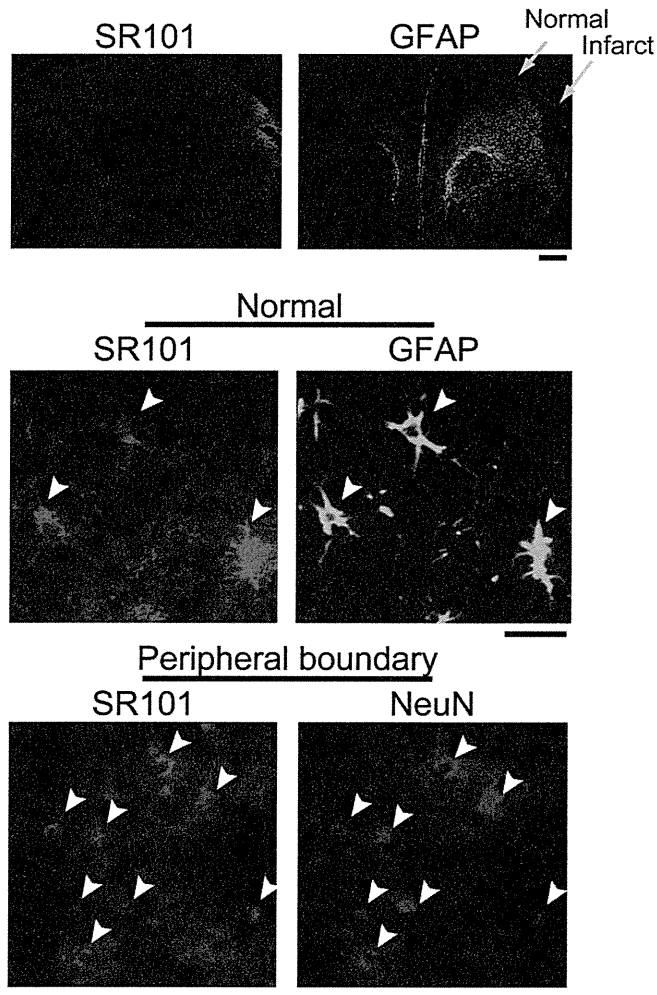

Fig. 8. Immunohistochemistry at the ischemic boundary on day 4 post-MCAO. On the nearside of the ischemic core (downward in the image), SR101-labeled cells (red) were also labeled with NeuN (blue), indicating that SR101 was taken up by neurons following ischemia. In contrast, co-localization of SR101-labeled cells with GFAP positive cells (green) was detected on the outside of ischemic core, indicating that all astroglia in the normal areas were labeled with SR101. Scale bar = 50 μm. (For interpretation of the references to colour in this figure legend, the reader is referred to the web version of this article.)

could be due to the different concentration of SR101 in the vessels and astroglia.

It was shown that injection of SR101 (10 μM of 5 μL or 10 μL) into extracellular space of hippocampus provoked seizure-like response of *in vivo* rats under ketamine/xylazine anesthesia (Kang et al., 2010). In the present study, we used relatively high-concentration of SR101 (5–10 mM in saline), but no detectable changes of behavior activity and evoked decrease of body weight were observed. Assuming that animal blood volume is 2 mL, the intraperitoneally injected SR101 (e.g., 0.2 mL) could be diluted approximately 10-fold in blood circulation. Furthermore, due to a presence of blood–brain barrier we assumed that < 10% of SR101 in blood was transported to tissue, and thus estimated concentration of SR101 in tissue could be equivalent or slightly higher than that of standard procedure that applied SR101 directly to the cortex (25–100 μM; Nimmerjahn et al., 2004). Nevertheless, following the injection of SR101, no detectable leakage of SR101 from blood to tissue was observed in the present study, which indicates that transportation of SR101 to astrocyte was regulated by its direct uptake from blood circulation. Furthermore, we observed no detectable differences of evoked blood flow response to whisker stimulation and animal locomotion in the animals subject to the SR101 injection (unpublished data), as compared to those of non-SR101 injected animals (Takuwa et al., 2011). These results suggest that intraperitoneal injection of SR101 (i.e., direct uptake by astrocyte) had minimum effects on the functions of neurons and vascular cells. These results are also in good agreement with a recent paper that showed that the interference of SR101 with neural excitability is not mediated by the SR101-loaded astrocytes (Kang et al., 2010).

In the MCAO animals, the image captured after MCAO showed poor depth penetration compared to the pre-MCAO, which could be due to changes of tissue optical properties, such as an increase in optical scattering and/or absorption evoked by ischemic injury. As was seen in the MRI experiments, MCAO induced tissue edema (both cytotoxic and vasogenic) in the MCA territory regions 24 h after the occlusion, which may cause the

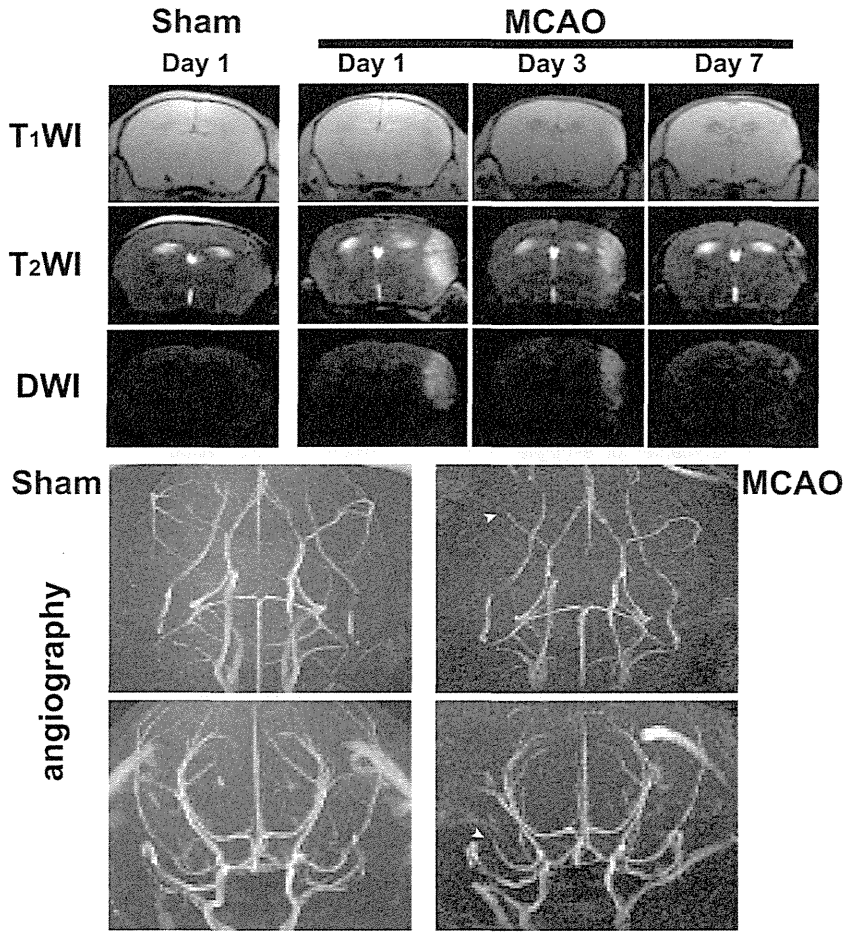

Fig. 9. *In vivo* MRI experiments in MCAO animals. The signal changes in the occluded side of the cortex was detected in both T_2- and diffusion-weighted MRI 1 day after MCAO, which was consistent over a period of the experiments up to 7 days from MCAO. No signal changes were evident in the sham-operated animal. The mean infarct volume in the MCAO animals calculated using T_2-weighted MRIs was $33.5 \pm 4.8\,mm^3$. The MCA was certainly occluded (5/5) and no reflow in the occluded side of MCA was seen in MR angiography (bottom, arrow head).

change of the tissue optical properties. Because we were not able to match the disturbed blood flow regions and the location of damaged microvascular networks in the obtained 3D microscopic images, an exact location of the ischemic penumbra cannot be identified. Nevertheless, we observed the labeling of neurons in areas of the ischemic boundary where the neighboring microvasculature was distorted, which implies that the ischemia-induced hypoxia opened neuronal hemichannels (Thompson et al., 2006). The results further allow the *in vivo* assessment of viability status in the ischemic zone. Taken together, the *in vivo* methods presented here will enable us to unravel the complex cellular events spatiotemporally evoked by an ischemic gradient from the core to peripheral boundary. With the repeated longitudinal imaging, future studies must establish a novel therapeutic approach to controlling a sequence of events at a defined time and space after cerebral ischemia.

Acknowledgements—The study was partly supported by Special Coordination Funds for Promoting Science and Technology and Kakenhi. Authors thank Sayaka Shibata, Misao Yoneyama, and Takeo Shimomura (Molecular Imaging Center, NIRS) for technical support of animal handling and MRI measurements.

REFERENCES

Abbott NJ, Rönnbäck L, Hansson E (2006) Astrocyte-endothelial interactions at the blood–brain barrier. Nat Rev Neurosci 7:41–53.

Carmignoto G, Gómez-Gonzalo M (2010) The contribution of astrocyte signalling to neurovascular coupling. Brain Res Rev 63:138–148.

del Zoppo GJ (2010) The neurovascular unit in the setting of stroke. J Intern Med 267:156–171.

del Zoppo GJ, Mabuchi T (2003) Cerebral microvessel responses to focal ischemia. J Cereb Blood Flow Metab 23:879–894.

Gordon GR, Choi HB, Rungta RL, Ellis-Davies GC, MacVicar BA (2008) Brain metabolism dictates the polarity of astrocyte control over arterioles. Nature 456:745–749.

Itoh Y, Toriumi H, Yamada S, Hoshino H, Suzuki N (2010) Resident endothelial cells surrounding damaged arterial endothelium reendothelialize the lesion. Arterioscler Thromb Vasc Biol 30:1725–1732.

Kafitz KW, Meier SD, Stephan J, Rose CR (2008) Developmental profile and properties of sulforhodamine 101–Labeled glial cells in acute brain slices of rat hippocampus. J Neurosci Methods 169:84–92.

Kang J, Kang N, Yu Y, Zhang J, Petersen N, Tian GF, Nedergaard M (2010) Sulforhodamine 101 induces long-term potentiation of intrinsic excitability and synaptic efficacy in hippocampal CA1 pyramidal neurons. Neuroscience 169:1601–1609.

Kleinfeld D, Mitra PP, Helmchen F, Denk W (1998) Fluctuations and stimulus-induced changes in blood flow observed in individual capillaries in layers 2 through 4 of rat neocortex. Proc Natl Acad Sci USA 95:15741–15746.

Mathiisen TM, Lehre KP, Danbolt NC, Ottersen OP (2010) The perivascular astroglial sheath provides a complete covering of the brain microvessels: an electron microscopic 3D reconstruction. Glia 58:1094–1103.

McCaslin AF, Chen BR, Radosevich AJ, Cauli B, Hillman EM (2011) In vivo 3D morphology of astrocyte-vasculature interactions in the somatosensory cortex: implications for neurovascular coupling. J Cereb Blood Flow Metab 31:795–806.

Motoike T, Loughna S, Perens E, Roman BL, Liao W, Chau TC, Richardson CD, Kawate T, Kuno J, Weinstein BM, Stainier DY, Sato TN (2000) Universal GFP reporter for the study of vascular development. Genesis 28:75–81.

Nimmerjahn A, Kirchhoff F, Kerr JN, Helmchen F (2004) Sulforhodamine 101 as a specific marker of astroglia in the neocortex in vivo. Nat Methods 1:31–37.

Park SH, Masamoto K, Hendrich K, Kanno I, Kim SG (2008) Imaging brain vasculature with BOLD microscopy: MR detection limits determined by in vivo two-photon microscopy. Magn Reson Med 59:855–865.

Paxinos G, Franklin KBJ The mouse brain in stereotaxic coordinates. Gulf Professional Publishing; 2004.

Rovainen CM, Woolsey TA, Blocher NC, Wang DB, Robinson OF (1993) Blood flow in single surface arterioles and venules on the mouse somatosensory cortex measured with videomicroscopy, fluorescent dextrans, nonoccluding fluorescent beads, and computer-assisted image analysis. J Cereb Blood Flow Metab 13:359–371.

Sarelius IH, Duling BR (1982) Direct measurement of microvessel hematocrit, red cell flux, velocity, and transit time. Am J Physiol 243:H1018–1026.

Seylaz J, Charbonné R, Nanri K, Von Euw D, Borredon J, Kacem K, Méric P, Pinard E (1999) Dynamic in vivo measurement of erythrocyte velocity and flow in capillaries and of microvessel diameter in the rat brain by confocal laser microscopy. J Cereb Blood Flow Metab 19:863–870.

Shannon C, Salter M, Fern R (2007) GFP imaging of live astrocytes: regional differences in the effects of ischaemia upon astrocytes. J. Anat. 210:684–692.

Straub SV, Nelson MT (2007) Astrocytic calcium signaling: the information currency coupling neuronal activity to the cerebral microcirculation. Trends Cardiovasc Med 17:183–190.

Takuwa H, Autio J, Nakayama H, Matsuura T, Obata T, Okada E, Masamoto K, Kanno I (2011) Reproducibility and variance of a stimulation-induced hemodynamic response in barrel cortex of awake behaving mice. Brain Res 1369:103–111.

Tamura A, Graham DI, McCulloch J, Teasdale GM (1981) Focal cerebral ischaemia in the rat: 1. Description of technique and early neuropathological consequences following middle cerebral artery occlusion. J Cereb Blood Flow Metab 1:53–60.

Thompson RJ, Zhou N, MacVicar BA (2006) Ischemia opens neuronal gap junction hemichannels. Science 312:924–927.

Tomita Y, Kubis N, Calando Y, Tran Dinh A, Méric P, Seylaz J, Pinard E (2005) Long-term in vivo investigation of mouse cerebral microcirculation by fluorescence confocal microscopy in the area of focal ischemia. J Cereb Blood Flow Metab 25:858–867.

Toriumi H, Tatarishvili J, Tomita M, Tomita Y, Unekawa M, Suzuki N (2009) Dually supplied T-junctions in arteriolo-arteriolar anastomosis in mice: key to local hemodynamic homeostasis in normal and ischemic states? Stroke 40:3378–3383.

Vérant P, Ricard C, Serduc R, Vial JC, van der Sanden B (2008) In vivo staining of neocortical astrocytes via the cerebral microcirculation using sulforhodamine B. J Biomed Opt 13:064028.

Zhuo L, Sun B, Zhang CL, Fine A, Chiu SY, Messing A (1997) Live astrocytes visualized by green fluorescent protein in transgenic mice. Dev Biol 187:36–42.

(Accepted 26 March 2012)
(Available online 16 April 2012)